Theory of resonant tunneling through a quantum wire

N. Mori,* P.H. Beton, J. Wang,† and L. Eaves
Department of Physics, University of Nottingham, Nottingham NG7 2RD, United Kingdom
(Received 29 June 1994; revised manuscript received 6 October 1994)

Quantum confined GaAs/AlAs resonant tunneling diodes with submicron lateral dimensions are studied theoretically using the transfer Hamiltonian formalism. It is shown that a high magnetic field normal to the current and parallel to the quantum wire cavity can be used to unambiguously identify the lateral quantum confinement. The current-voltage characteristics for other magnetic field orientations are also discussed.

I. INTRODUCTION

Since the seminal work of Chang, Esaki, and Tsu,[1] resonant tunneling of electrons through a double-barrier quantum well has been extensively studied. Recent developments in microfabrication technology have made it possible to produce resonant tunneling diodes (RTD's) with cavities in the form of quantum dots or wires, i.e., zero-dimensional (0D) or one-dimensional (1D) RTD's. Many researchers have investigated effects of quantum confinement on resonant tunneling in such structures experimentally[2–16] and theoretically.[17–24]

Reed *et al.* observed a series of peaks superimposed on the negative-differential-resistance peak in a submicron RTD fabricated using electron-beam lithography and reactive-ion etching.[2] The observed structure was attributed to resonant tunneling through the discrete quasibound states in the quantum well. In the absence of scattering, additional structure is not expected to appear in a RTD when the lateral (parallel to the heterointerface) confining potential is the same throughout the diode.[17] Bryant has argued that the observed structure is caused by the extreme difference in the emitter and the well confining potentials which enables subband mixing at the interfaces,[19] or it occurs when the discrete states in the well are resonant with the emitter Fermi level rather than the band edge of the emitter subbands.[24] A similar submicron RTD structure was used to study the tunneling time, the inelastic scattering time, and the transmission probability, where a sharp steplike structure was observed well below the main peak in the current-voltage characteristics $I(V)$.[5] Steplike features between threshold and main peak voltage in $I(V)$ were also reported.[6]

Tarucha *et al.* prepared one- and zero-dimensional RTD's whose lateral confinement was imposed by a focused Ga ion beam, and observed fine structure in the $I(V)$, which was assigned to mixing of even- or odd-parity subbands in the well with subbands of the same parity in the emitter.[4] The emitter confining potential dependence of $I(V)$ of 1D RTD's was also reported.[7] By analyzing a series of current peaks at the onset of tunneling current in 0D RTD's, Tarucha *et al.* suggested that the magnitude of peak current is defined by the degeneracy of the zero-dimensional level in the well.[8] Guéret *et al.* reported fine structure observed in the $I(V)$ of a gated resonant tunneling diode and argued that the observed structure gives direct proof of the quantum size effect.[10]

However, more recent work has shown that additional peaks in $I(V)$ may arise from a completely different mechanism.[9,25] Shallow donors, which are incorporated into the quantum well either unintentionally[9] or intentionally,[16] give rise to a localized preferential current path which causes subthreshold peaks in the $I(V)$. The appearance of additional structure in $I(V)$ of small area diodes, therefore, cannot be taken in itself as conclusive evidence for lateral quantum confinement.[14]

In this paper, we investigate theoretically resonant tunneling in 1D RTD's. In particular, we try to clarify effects of a magnetic field applied perpendicular to the current direction, which has been experimentally studied by using a structure of RTD with submicron lateral dimensions,[26,27] and show that a high magnetic field may be used to unambiguously identify the effects of lateral quantum confinement.

The organization of the present paper is as follows. In Sec. II, we present a model for the 1D RTD used for the experiments of Ref. 26 and the electronic states under applied magnetic field. Then the tunneling current is calculated by using the transfer Hamiltonian formalism, where lateral motion of electrons in the emitter is assumed to be free. The numerical results giving the tunneling current is presented in Sec. III. In Sec. IV, the effect of emitter confinement is discussed. A summary and discussion are given in Sec. V. Throughout this paper, we set $\hbar = 1$.

II. FORMALISM

A. Sample structure

A schematic diagram of the device used for the experiments[26] is shown in Fig. 1(a) together with the coordinate axes for the following discussion. The active area of the device is the region of overlap of two GaAs bars, one ($\ell_t = 0.5\,\mu$m) etched in the top contact layer and the other ($\ell_b = 1.0\,\mu$m) in the bottom contact layer. The sidewall depletion is $\sim 0.2\,\mu$m for each edge,[27] and the dimensions of the active conducting region is

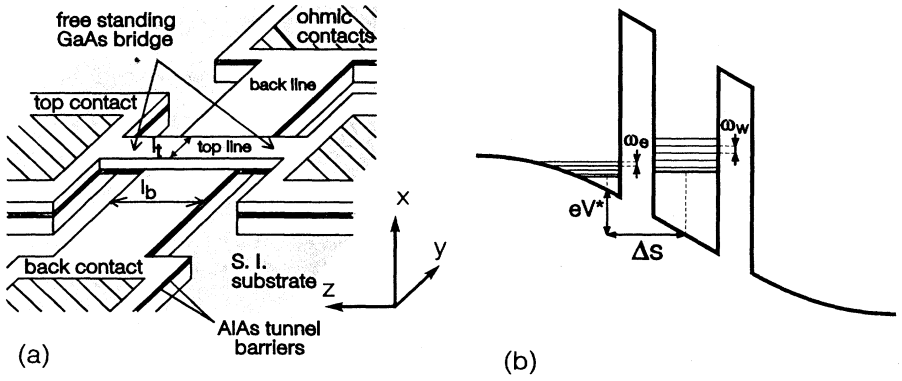

FIG. 1. Schematic diagrams of the GaAs/AlAs resonant tunneling diode (a) and the conduction band profile (b). The active area of the device is the region of overlap of two GaAs bars, one (thickness ℓ_t) etched in the top contact layer and the other (thickness ℓ_b) in the bottom contact layer.

$\sim 100\,\text{nm} \times 600\,\text{nm}$. The device is, therefore, considered to be a short quantum wire and electrons tunnel between 1D states formed in the emitter and the well. The $I(V)$ have been measured in forward bias where electrons flow from the bottom contact to the top contact, and the experimental results are described in Ref. 26.

B. Model

We use the effective mass approximation and the transfer Hamiltonian formalism to calculate the tunneling current for the 1D RTD assuming that the current is limited by the emitter barrier. Electronic states of the emitter and well regions are considered separately. In principle, the confining potentials could be calculated, however, this requires too much computational time since a RTD is an open boundary system.[28] In this paper, we consider fundamental features of $I(V)$ in 1D RTD's, especially those at high magnetic field. We, therefore, use a simple model for emitter and well confining potentials which gives analytical electronic states even under magnetic field and is considered to be a good approximation for a qualitative discussion.

We assume that electrons are free along the z direction and confining potentials of the emitter and the well are, respectively, given by

$$V_e(x,y) = \tfrac{1}{2}m\Omega_e^2(x+\Delta s)^2 + \tfrac{1}{2}m\omega_e^2 y^2 \ , \tag{2.1}$$

$$V_w(x,y) = \tfrac{1}{2}m\Omega_w^2 x^2 + \tfrac{1}{2}m\omega_w^2 y^2 \ , \tag{2.2}$$

where the x axis is defined to be the growth direction, and y and z are, respectively, perpendicular and parallel to the long axis of the quantum wire [see Fig. 1(a)]. Δs is the distance between the emitter and the well.

The lateral confinement along the y direction is caused by the sidewall depletion and the confining potential is approximated by a parabolic potential. The strengths are expressed by the parameters ω_e and ω_w for the emitter and the well states, respectively. Because of the asymmetric device structure, the degree of confinement is expected to be different in the emitter and the well. For forward bias, where electrons flow from the bottom contact to the top contact, $\omega_e < \omega_w$, and for reverse bias, $\omega_e > \omega_w$. In this section, we consider $I(V)$ for forward bias and we assume $\omega_e = 0$ for simplicity. The effect of finite ω_e and $I(V)$ for reverse bias are considered in the following sections.

The confinement along the x direction is due to the heterostructure, and for the well is close to a square potential and for the emitter is similar to a triangle potential. The relative strength is an important factor even for a qualitative discussion. However, the detailed shape of the confining potential is not so crucial provided the transfer matrix element is properly approximated. We, therefore, assume simple parabolic confining potentials along the growth direction. The strengths are expressed by the parameters Ω_e and Ω_w for the emitter and the well, respectively. The actual well width of 90 Å implies $\Omega_w > \Omega_e$.

C. Magnetic field parallel to the long axis ($\omega_e = 0$)

1. *Electronic states*

For a magnetic field oriented in the z direction, the single particle Hamiltonian for the emitter, $\mathcal{H}_e$, can be written, using the Landau gauge $\mathbf{A} = (0, Bx, 0)$, as

$$\mathcal{H}_e = \frac{p_x^2}{2m} + \frac{1}{2m}(p_y + eBx)^2 + \frac{p_z^2}{2m} + \tfrac{1}{2}m\Omega_e^2(x+\Delta s)^2. \tag{2.3}$$

In the $\{x,y,z\}$ representation, the eigenenergies and the corresponding eigenfunctions are given by

$$E^e_{ik_yk_z} = (i+\tfrac{1}{2})\widetilde{\Omega}_e + \frac{1}{2M_e}(k_y - eB\Delta s)^2 + \frac{k_z^2}{2m} \tag{2.4}$$

and

$$\Psi^e_{ik_yk_z}(x,y,z) = \phi_i(\widetilde{L}_e; x+\Delta s - X_e)e^{ik_y y}e^{ik_z z} \tag{2.5}$$

where $\widetilde{\Omega}_e = (\Omega_e^2+\omega_c^2)^{1/2}$, $\omega_c = eB/m$, $M_e = m(\widetilde{\Omega}_e/\Omega_e)^2$ $\widetilde{L}_e = (m\widetilde{\Omega}_e)^{-1/2}$, $X_e = -(\omega_c/(m\widetilde{\Omega}_e^2))(k_y - eB\Delta s)$, and $\phi_i(\ell;x)$ is the simple harmonic-oscillator-like solution

$(i = 0, 1, 2, \ldots,)$.[29] Since $\Omega_e \sim 20\,\text{meV}$ for the device used for the experiments, only the lowest level ($i = 0$) is occupied at low temperature. We, therefore, consider only the lowest level in the following analysis. The energy level shows diamagnetic shift for lower magnetic field as $\propto \omega_c^2/(2\Omega_e)$.

For the well, the Hamiltonian is

$$\mathcal{H}_w = \frac{p_x^2}{2m} + \frac{1}{2m}(p_y + eBx)^2 + \frac{p_z^2}{2m} + \tfrac{1}{2}m\Omega_w^2 x^2 + \tfrac{1}{2}m\omega_w^2 y^2 \tag{2.6}$$

The energies and the eigenfunctions can be written, in the $\{x, p_y, z\}$ representation, as[30]

$$E^w_{ijk_z} = (i + \tfrac{1}{2})\omega_+ + (j + \tfrac{1}{2})\omega_- + \frac{k_z^2}{2m} \tag{2.7}$$

and

$$\Psi^w_{ijk_z}(x, p_y, z) = \phi_i(\ell_+; x')\,\phi_j(\ell_-; q_y')\,e^{ik_z z}\ , \tag{2.8}$$

where the coordinates $[x, q_y \equiv p_y/(m\omega_w)]$ are rotated to (x', q_y') by the angle of rotation $\theta = \frac{1}{2}\tan^{-1}[2\omega_c\omega_w/(\Omega_w^2 - \omega_w^2 + \omega_c^2)]$, and $2\omega_\pm^2 = \Omega_w^2 + \omega_w^2 + \omega_c^2 \pm [(\Omega_w^2 - \omega_w^2 + \omega_c^2)^2 + 4\omega_w^2\omega_c^2]^{1/2}$ and $\ell_\pm = (m\omega_\pm)^{-1/2}$. For the real device, $\Omega_w \sim 80\,\text{meV}$ and ω_w is considered to be a few meV. Therefore, we may neglect ω_w/Ω_w as compared with unity in the lowest order of ω_w/Ω_w, and we have

$$E^w_{ijk_z} = (i + \tfrac{1}{2})\widetilde{\Omega}_w + (j + \tfrac{1}{2})\hat{\omega}_w + \frac{k_z^2}{2m} \tag{2.9}$$

and

$$\Psi^w_{ijk_z}(x, p_y, z) = \phi_i(\widetilde{L}_w; x)\,\phi_j(\hat{\ell}_w; q_y)\,e^{ik_z z}. \tag{2.10}$$

$\widetilde{\Omega}_w = (\Omega_w + \omega_c)^{1/2}$, $\hat{\omega}_w = \omega_w(\Omega_w/\widetilde{\Omega}_w)$, $\widetilde{L}_w = (m\widetilde{\Omega}_w)^{-1/2}$, and $\hat{\ell}_w = (m\hat{\omega}_w)^{-1/2}$. Since the resonant peak involving the ground state ($i = 0$) was observed in the experiments, we set $i = 0$ in the following analysis. The energy level depends on B as $\widetilde{\Omega}_w$ and shows diamagnetic shift for lower magnetic fields as $\propto \omega_c^2/(2\Omega_w)$, which is smaller than that in the emitter because $\Omega_w > \Omega_e$.

2. *Tunneling current*

When the tunneling current I is limited by the emitter barrier, I is given by[31]

$$I = 2e\sum_{k_yk_z}\sum_{jk_z'}|T_{jk_z',k_yk_z}|^2\int\frac{d\varepsilon}{2\pi}A_e(k_yk_z;\varepsilon) \times A_w(jk_z';\varepsilon + eV^*)f(\varepsilon)\ , \tag{2.11}$$

where we neglect charge accumulation in the well and assume that the final state in the collector is empty. V^* is the effective applied voltage between the emitter and the well [see Fig. 1(b)], $f(\varepsilon)$ is the electron distribution function in the emitter, T_{jk_z',k_yk_z} is the tunneling matrix elements between (k_yk_z) states in the emitter and (jk_z') states in the well, and $A_e(k_yk_z;\varepsilon)$ and $A_w(jk_z;\varepsilon)$ are the spectral density functions in the emitter and the well, respectively. The tunneling matrix elements are given by

$$|T_{jk_z',k_yk_z}|^2 = t^2\Phi_j^2(\ell_w^{-2}\hat{\ell}_w; k_y)\delta_{k_z,k_z'}\ , \tag{2.12}$$

where $\Phi_j(\ell^{-1}; k)$ is the Fourier transform of $\phi_j(\ell; x)$,[32] $\ell_w = (m\omega_w)^{-1/2}$, and t is the one-dimensional Bardeen transfer matrix element which is evaluated at some point x_0 in the emitter barrier:

$$t = \frac{1}{2m}\left\{\chi_e(x)\frac{\partial\chi_w(x)}{\partial x} - \frac{\partial\chi_e(x)}{\partial x}\chi_w(x)\right\}\Bigg|_{x=x_0}\ . \tag{2.13}$$

$\chi_e(x)$ and $\chi_w(x)$ are the wave functions associated with the quantized x motion in the emitter and the well, respectively. This parameter, however, determines the absolute value of I and is nearly independent of V^* and B. We, therefore, assume that t is constant and independent of V^* and B.

Assuming a simple Lorentzian spectral function of characteristic width Γ in Eq. (2.11), we have

$$\frac{I}{I_0} = \ell_w\sum_j\int\frac{dk_y}{2\pi}\int\frac{dk_z}{2\pi}\Phi_j^2(\ell_w^{-2}\hat{\ell}_w; k_y) \times\frac{\Gamma^2}{(E^e_{0k_yk_z} + eV^* - E^w_{0jk_z})^2 + \Gamma^2}f(E^e_{0k_yk_z})\ , \tag{2.14}$$

where $I_0 = 4et^2L_z/(\Gamma\ell_w)$ and we have restored the length of quantum wire along the z direction, L_z. Γ is a parameter characterizing the energy broadening. Γ has a contribution for the intrinsic widths Γ_e and Γ_w of the states in the emitter and the well. Moreover, a contribution is also expected from inhomogeneous broadening in the conduction band minimum along the length of the wire. The current I depends on temperature through the distribution function $f(\varepsilon)$ and Γ. In the following discussion, we consider low temperature $I(V)$ and use zero temperature $f(\varepsilon)$ for simplicity.

When the Fermi energy ε_F in the emitter is assumed to be independent of magnetic field, Eq. (2.14) is reduced to

$$\frac{I}{I_0} = \frac{\ell_w}{\pi}\frac{\Omega_e}{\widetilde{\Omega}_e}\sum_j\int_{-k_F}^{k_F}\frac{dk_y}{2\pi}(k_F^2 - k_y^2)^{1/2} \times\Phi_j^2(\ell_w^{-2}\hat{\ell}_w; k_y + eB\Delta s)\frac{\Gamma^2}{(\varepsilon_{k_y} + eV^* - \varepsilon_j)^2 + \Gamma^2}. \tag{2.15}$$

k_F is the Fermi wave vector in the emitter, $\varepsilon_{k_y} = k_y^2/(2M_e) + \frac{1}{2}\widetilde{\Omega}_e$, and $\varepsilon_j = (j + \frac{1}{2})\hat{\omega}_w + \frac{1}{2}\widetilde{\Omega}_w$.

The current I is mainly determined by two factors: the energy matching condition, $\Gamma^2/(\Delta\varepsilon_{jk_y}^2 + \Gamma^2)$ (where $\Delta\varepsilon_{jk_y}$ is the energy difference between the emitter and the well, and is given by $\varepsilon_{k_y} + eV^* - \varepsilon_j$), and the tunneling matrix elements along the y direction, $\Phi_j^2(k_y)$. The applied field B affects the energy matching condition mainly through the difference in the diamagnetic shifts in the emitter and the well states, and the tunneling matrix elements by changing their argument by $eB\Delta s$.

D. Magnetic field perpendicular to the long axis ($\omega_e = 0$)

1. Electronic states

Under the magnetic field oriented in the y direction, $\mathbf{A}$ is given by $(0, 0, -Bx)$ in the Landau gauge, and the Hamiltonian for the emitter can be written as

$$\mathcal{H}_e = \frac{p_x^2}{2m} + \frac{p_y^2}{2m} + \frac{1}{2m}(p_z - eBx)^2 + \tfrac{1}{2}m\Omega_e^2(x + \Delta s)^2. \tag{2.16}$$

The energies and the corresponding eigenfunctions are

$$E^e_{ik_yk_z} = (i + \tfrac{1}{2})\widetilde{\Omega}_e + \frac{k_y^2}{2m} + \frac{1}{2M_e}(k_z + eB\Delta s)^2 \tag{2.17}$$

and

$$\Psi^e_{ik_yk_z}(x, y, z) = \phi_i(\widetilde{L}_e; x + \Delta s - X_e)\, e^{ik_y y}\, e^{ik_z z}\ , \tag{2.18}$$

with $X_e = [\omega_c/(m\widetilde{\Omega}_e^2)](k_z + eB\Delta s)$.

For the well, the Hamiltonian is

$$\mathcal{H}_w = \frac{p_x^2}{2m} + \frac{p_y^2}{2m} + \frac{1}{2m}(p_z - eBx)^2 + \tfrac{1}{2}m\Omega_w^2 x^2 + \tfrac{1}{2}m\omega_w^2 y^2 \tag{2.19}$$

and, the energies and eigenfunctions are given by

$$E^w_{ijk_z} = (i + \tfrac{1}{2})\widetilde{\Omega}_w + (j + \tfrac{1}{2})\omega_w + \frac{k_z^2}{2M_w} \tag{2.20}$$

and

$$\Psi^w_{ijk_z}(x, y, z) = \phi_i(\widetilde{L}_w; x - X_w)\, \phi_j(\ell_w; y)\, e^{ik_z z} \tag{2.21}$$

with $M_w = m(\widetilde{\Omega}_w/\Omega_w)^2$ and $X_w = (\omega_c/(m\widetilde{\Omega}_e^2))k_z$.

2. Tunneling current

The tunneling current under the magnetic field applied perpendicular to the long axis of the quantum wire can be calculated by the same way of parallel field case, and we have

$$\frac{I}{I_0} = \ell_w \sum_j \int \frac{dk_y}{2\pi} \int \frac{dk_z}{2\pi} \Phi_j^2(\ell_w^{-1}; k_y) \times \frac{\Gamma^2}{(\varepsilon_{k_yk_z} + eV^* - \varepsilon_{j,k_z - eB\Delta s})^2 + \Gamma^2} f(\varepsilon_{k_yk_z})\ , \tag{2.22}$$

where $\varepsilon_{k_yk_z} = k_y^2/(2m) + k_z^2/(2M_e) + \frac{1}{2}\widetilde{\Omega}_e$ and $\varepsilon_{jk_z} = (j + \frac{1}{2})\omega_w + k_z^2/(2M_w) + \frac{1}{2}\widetilde{\Omega}_w$.

For $B \parallel y$, electron motion along the y axis is not affected by B during the tunneling process. Therefore, the matrix elements $\Phi_j^2(k_y)$ in I are independent of B. On the other hand, the energy matching condition is strongly affected by B because the energy difference, $\Delta\varepsilon_{jk_yk_z} = \varepsilon_{k_yk_z} + eV^* - \varepsilon_{j,k_z - eB\Delta s}$, explicitly depends on B. This causes peak shift and broadening of the resonance at high magnetic field, which has been thoroughly studied in conventional large area diodes.[33–36]

III. NUMERICAL RESULTS

Figure 2 shows the calculated currents as a function of ΔE $[= eV^* - \frac{1}{2}(\Omega_w + \omega_w - \Omega_e)]$ in the presence of a magnetic field perpendicular [Fig. 2(a)] or parallel [Fig. 2(b)] to the long axis of the wire. At $\Delta E = 0$, the lowest level in the emitter is aligned to that in the well for $B = 0$. The following parameters were used for the calculation : $\Omega_e = 20$ meV, $\Omega_w = 80$ meV, $\omega_w = 3.5$ meV, $\varepsilon_F = 6$ meV, $\Gamma = 2$ meV, and $\Delta s = 200$ Å. The choice of the parameters is justified in Ref. 26 excepting Γ, which we treat as a fitting parameter, and Γ dependence of $I(V)$ is discussed in the next section. There is a good agreement between the calculated and experimental curves (see Figs. 2 and 3 in Ref. 26), except for the high field weak modulation observed for $B \parallel y$, which is caused by the discreetness of the emitter states, therefore, the feature is not observed for continuum ($\omega_e = 0$) emitter states, and will be explained in the next section.

The effect of field for $B \parallel y$ is similar to that for large area diodes as was mentioned above. Because of the explicit B dependence of energy difference $\Delta\varepsilon_{jk_yk_z} = \varepsilon_{k_yk_z} + eV^* - \varepsilon_{j,k_z - eB\Delta s}$, the voltage threshold for resonant tunneling shifts to a higher value with increasing B followed by a broadening of the resonance.[33–36]

For parallel high field, $B \parallel z$, the coupling between the emitter and the well states is strongly modified as $\Phi_j^2(k_y + eB\Delta s)$. Figure 3 shows $\Phi_j^2(k_y)$ up to $j = 15$. The

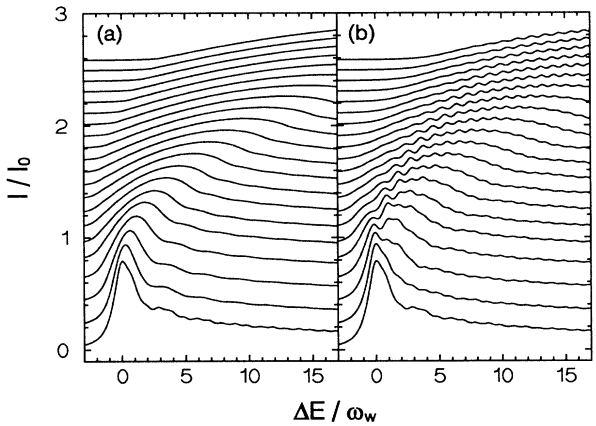

FIG. 2. Calculated plots of tunneling currents as a function of effective applied bias ΔE in the presence of a magnetic field between $\omega_c = 0$ meV (lowest curve) and $\omega_c = 20$ meV (top curve) in 1 meV steps. The field is oriented normal to the current direction and either perpendicular (a) or parallel (b) to the long axis of the quantum wire. The emitter confinement along the y direction is neglected ($\omega_e = 0$). $\Delta E = 0$ corresponds to an applied voltage which aligns the lowest levels of the emitter and the well at $B = 0$. Parameters are discussed in the text.

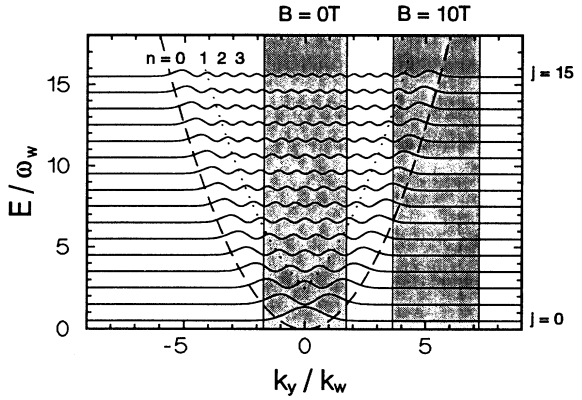

FIG. 3. Plots of probability density $\Phi_j^2(k_y)$ versus k_y for laterally bound states in the quantum well for $j = 0 \sim 15$ (solid lines), the dispersion of the emitter states (broken line), and the locus of the $n = 1$ maxima (dotted line). Also shown (shaded) is the integration range for Eq. (2.15) for $B = 0\,\mathrm{T}$ and $10\,\mathrm{T}$. The horizontal axis is in units $k_w = (m\omega_w)^{1/2}$. There are N $(= [j/2] + 1)$ maxima in $\Phi_j^2(k_y)$ lying in the range of $k_y \leq 0$ (or $k_y \geq 0$) labeled $n = 0, 1, 2, \ldots$, for the $j = 15$ curve.

high energy states have pronounced maxima in $\Phi_j^2(k_y)$ at a value $k_{j,\max}$ $(= [2m(j + \frac{1}{2})\omega_w]^{1/2})$ and $-k_{j,\max}$. As B is increased, these maxima are the only features in $\Phi_j^2(k_y)$ which remain within the integration range of $-k_F + eB\Delta s \leq k_y \leq k_F + eB\Delta s$ for $\Phi_j(k_y)$. This is true, for example, for states $j = 0 \sim 11$ at $B = 10\,\mathrm{T}$ (see Fig. 3). At this value of B tunneling through states $j = 6 \sim 11$, therefore, results in one clear isolated peak $I(V)$. A further increase in B moves the integration range beyond $k_{j,\max}$ and the tunneling current through the jth state falls to zero (this is true for $j = 0 \sim 5$ at $B = 10\,\mathrm{T}$, see Fig. 3). This corresponds to the high field amplitude dependence of observed peaks. The shift of a given peak to lower voltage is due to the difference in the diamagnetic shifts in the emitter and the well.

The amplitude dependence for $B = 0$ is more complicated, and it can be explained as follows. Peaks in $I(V)$ occur when the energy matching condition $\Delta\varepsilon_{jk_y}(V^*) \sim 0$ is met. There are N $(= [j/2] + 1)$ maxima in $\Phi_j^2(k_y)$ lying in the range of $k_y \leq 0$ (or $k_y \geq 0$). Therefore a given jth state will give rise to at most N peaks in $I(V)$. The voltage position of these N peaks, V_{jn}^* $(n = 0, 1, \ldots, N-1)$, is given by $\Delta\varepsilon_{jk_{jn}}(V_{jn}^*) \sim 0$ with k_{jn} being the position of the nth maximum in $\Phi_j^2(k_y)$ (see Fig. 3). These peaks correspond to the weak structure observed in the calculated curve. The voltage (V^*) separation is smaller than the corresponding level spacing, ω_e, for finite Fermi energy of $\varepsilon_F \gtrsim \omega_w$, because $|k_{(j+1),n}| > |k_{jn}|$ implies $V_{(j+1),n}^* - V_{jn}^* < \omega_e/e$.

The peaks in $I(V)$ corresponding to the nth maximum in $\Phi_j^2(k_y)$ but from different subbands (different index j) tend to occur at approximately the same voltage. This is because the locus of the nth maxima in (ε, k_y) space (see Fig. 3 in which the locus of the $n = 1$ maxima is shown as a dotted line) is approximately parallel to the dispersion of the emitter states. Therefore, these peaks tend to merge and form a single peak for appropriate Γ and ε_F. This is the origin of the background modulation in the calculated curve, and corresponds to the stronger peaks (see peaks labeled A–F in Fig. 2 in Ref. 26) observed in the experiments (the detailed structure is different between the experimental and calculated curves since $\omega_e > 0$ for the actual device as will be discussed in the next section), so we can associate the observed peaks A, B, C, ..., with $n = 0, 1, 2, \ldots$, maxima. The spacing in V^* is larger than ω_w/e and $\sim 2\omega_w/e$ because the peaks involving nth maximum appear for $\Delta E \geq 2n\omega_w$.

IV. EFFECTS OF FINITE CONFINEMENT

A. Magnetic field parallel to the long axis ($\omega_e > 0$)

For finite emitter lateral confining potential ($\omega_e > 0$) the emitter states can be given analytically as for the well states, and the current can be written as

$$\frac{I}{I_0} = \frac{1}{\pi}\sum_{ij} k_{Fi}\ell_w M_{ij}^2(eB\Delta s)\frac{\Gamma^2}{(\varepsilon_i + eV^* - \varepsilon_j)^2 + \Gamma^2} \tag{4.1}$$

for $B \parallel z$, where $k_{Fi} = \left\{2m[\varepsilon_F - (i + \frac{1}{2})\hat{\omega}_e]\right\}^{1/2}$, $\varepsilon_i = (i + \frac{1}{2})\hat{\omega}_e + \frac{1}{2}\widetilde{\Omega}_e$, $\varepsilon_j = (j + \frac{1}{2})\hat{\omega}_w + \frac{1}{2}\widetilde{\Omega}_w$, and

$$M_{ij}(eB\Delta s) = \int \frac{dk_y}{2\pi}\Phi_i(\ell_e^{-2}\hat{\ell}_e; k_y - eB\Delta s)\Phi_j(\ell_w^{-2}\hat{\ell}_w; k_y) \tag{4.2}$$

with $\ell_e = (m\omega_e)^{-1/2}$.

B. Magnetic field perpendicular to the long axis ($\omega_e > 0$)

For $B \parallel y$, the current is given by

$$\frac{I}{I_0} = \ell_w \sum_{ij} m_{ij}^2 \int_{-k_{Fi}}^{k_{Fi}} \frac{dk_z}{2\pi} \times \frac{\Gamma^2}{(\varepsilon_{ik_z} + eV^* - \varepsilon_{j,k_z - eB\Delta s})^2 + \Gamma^2}\,, \tag{4.3}$$

with $k_{Fi} = \left\{2M_e[\varepsilon_F - (i + \frac{1}{2})\omega_e]\right\}^{1/2}$, $\varepsilon_{ik_z} = (i + \frac{1}{2})\omega_e + k_z^2/(2M_e) + \frac{1}{2}\widetilde{\Omega}_e$, $\varepsilon_{jk_z} = (j + \frac{1}{2})\omega_w + k_z^2/(2M_w) + \frac{1}{2}\widetilde{\Omega}_w$, and

$$m_{ij} = \int \phi_i(\ell_e; y)\phi_j(\ell_w; y)dy. \tag{4.4}$$

C. Dependence of $I(V)$ on emitter confinement

Figure 4 shows the calculated tunneling currents as a function of effective applied voltage V^* for various values of ω_e (other parameters are the same as those for Fig. 2)

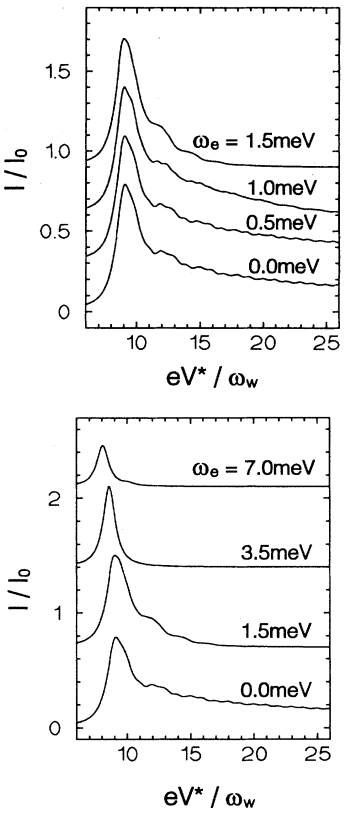

FIG. 4. Calculated plots of zero field tunneling currents as a function of effective applied voltage V^* for various values of lateral emitter confining energy ω_e. (a) $\omega_e = 0$, 0.5, 1, 1.5 meV and (b) $\omega_e = 0$, 1.5, 3.5, 7 meV (from bottom to top). The lateral confining energy of the well, ω_w, is 3.5 meV.

at zero field. For $\omega_e < \omega_w$ [Fig. 4(a)], we find that the $I(V)$ changes gradually as ω_e: the finite ω_e makes the stronger series clearer and weakens the smaller peaks, and the spacing of the stronger series becomes shorter as ω_e increases. These features are essentially understood from the fact that $I(V)$ has no peaks other than the main resonance for $\omega_e \sim \omega_w$,[17] and a detailed discussion about the change in the $I(V)$ will be given later. A further increase in ω_e beyond $\omega_e \sim \omega_w$ results in a lower peak current together with much weaker additional structure than that for $\omega_e < \omega_w$ [see $I(V)$ for $\omega_e = 7$ meV in Fig. 4(b)]. These features are consistent with the experimental $I(V)$ for reverse bias,[27] where ω_e is considered to be stronger than ω_w.

D. Dependence of $I(V)$ on level width

Before studying the magnetic field dependence of $I(V)$ for finite ω_e, we discuss the dependence of $I(V)$ on Γ, because Γ is the only parameter that we used as a fitting parameter. Figure 5 shows zero field $I(V)$ for $\omega_e = 1.5$ meV (Ref. 26) as a function of ΔE [$= eV^* - \frac{1}{2}(\Omega_w + \omega_w - \Omega_e - \omega_e)$] for $\Gamma = 1 \sim 2.5$ meV. Since the stronger series cannot be clearly identified for $\Gamma \lesssim 1$ meV, an appropriate finite Γ ($\simeq 1.5$ meV) is essential for the qualitative agreement between the experimental and the theoretical $I(V)$. For larger Γ, the stronger series of peaks is still observed but the weaker series is no longer resolved for $\Gamma \gtrsim 2$ meV. This should correspond to the observed temperature dependence of $I(V)$ (see Ref. 26) because we can expect larger Γ for higher temperature.

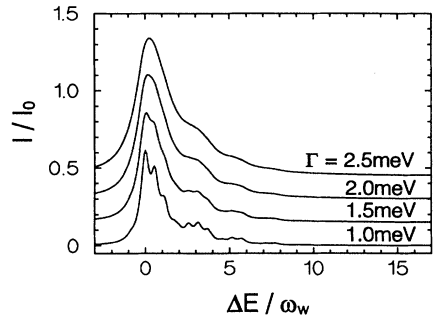

FIG. 5. Calculated plots of zero field tunneling currents as a function of effective applied bias ΔE for $\Gamma = 1$, 1.5, 2.0, 2.5 meV (from bottom to top). The lateral confining energy of the well, ω_w, is 3.5 meV, and that of the emitter, ω_e, is 1.5 meV.

E. Dependence of $I(V)$ on magnetic field

Figure 6 shows the calculated currents for finite ω_e as a function of ΔE in the presence of a magnetic field perpendicular [Fig. 6(a)] or parallel [Fig. 6(b)] to the long axis of the wire. The following parameters were

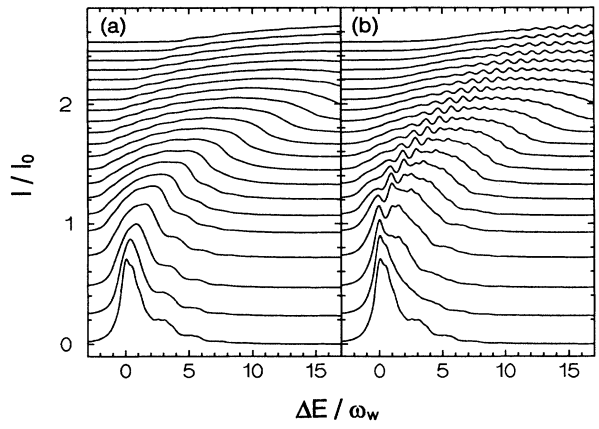

FIG. 6. Calculated plots of tunneling currents as a function of effective applied bias ΔE in the presence of a magnetic field between $\omega_c = 0$ meV (lowest curve) and $\omega_c = 20$ meV (top curve) in 1 meV steps. The field is oriented normal to the current direction and either perpendicular (a) or parallel (b) to the long axis of the quantum wire. The lateral confining energy of the emitter, ω_e, is 1.5 meV. $\Delta E = 0$ corresponds to an applied voltage which aligns the lowest levels of the emitter and the well at $B = 0$. Parameters are discussed in the text.

used for the calculation : $\Omega_e = 20\,\text{meV}$, $\Omega_w = 80\,\text{meV}$, $\omega_e = 1.5\,\text{meV}$, $\omega_w = 3.5\,\text{meV}$, $\varepsilon_F = 6\,\text{meV}$, $\Gamma = 1.5\,\text{meV}$, and $\Delta s = 200\,\text{Å}$. There is no qualitative difference between Fig. 2 for $\omega_e = 0$ and Fig. 6 for $\omega_e = 1.5\,\text{meV}$ except for the high field weak modulation observed for perpendicular field $B \parallel y$.

Figure 7 shows $I(V)$ for $B = 0\,\text{T}$ and $B = 6\,\text{T}$ (applied parallel to the long axis of the wire) together with $k_{Fi}M_{ij}^2(eB\Delta s)$ which corresponds to the contribution to the current from individual transitions between the ith state in the emitter and the jth state in the well [see Eq. (4.1)]. For zero field, the peak corresponding to peak A in the experimental data[26] is found to be composed of transitions between states with the same index, i.e., $(i,j) = (0,0)$, $(1,1)$, $(2,2)$, and $(3,3)$. We do not see any transitions for $i > 3$, because there are only four levels below the Fermi level in the emitter.[26] The next sequence of transitions which occur are $(0,2)$, $(1,3)$, $(2,4)$, and $(3,5)$, in which the change of index $j - i = 2$, followed by sequences for which $j - i = 4, 6, \ldots$. Note that for zero field only parity conserving transitions are allowed [$M_{ij}(0) = 0$ for $j - i =$ odd integer][4] and we do not observe transitions for $j - i =$ odd integer. The effect of broadening is to merge these sets of transitions so that the peaks that are most clearly resolved arise from the sets of transitions $j - i = 2n$ $(n = 0, 1, 2, \ldots,)$ for $\varepsilon_F \lesssim 2\omega_w$ corresponding to the peaks involving nth maximum in $\Phi_j^2(k_y)$ in the limit $\omega_e \to 0$ (both of them appear for $\Delta E \geq 2n\omega_w$) and peaks A–F in the experimental data. The voltage (V^*) separation of these peaks is, therefore, $\sim 2\omega_w/e$. This result shows that additional strong peaks may be observed in $I(V)$ for zero field but these peaks cannot be directly associated with resonant tunneling via particular quantized levels in the well. The weak structure is originated in the individual transitions and the voltage separation is $(\omega_w - \omega_e)/e$ except for the separation between the peaks involving different n sequences.

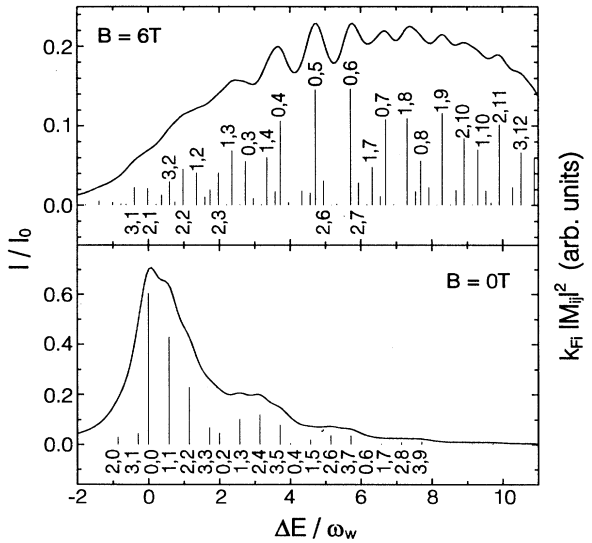

FIG. 7. Calculated $I(V)$ for $B = 0\,\text{T}$ and $6\,\text{T}$ (applied parallel to the long axis of the wire) together with the quantity $k_{Fi}M_{ij}^2(eB\Delta s)$ which is proportional to the current flowing between the ith state in the emitter and the jth state in the well. The transitions are classified by the pair of integers i, j. For $B = 0\,\text{T}$ the stronger peaks comprise the sets of parity conserving transitions $j - i = 2n$ $(n = 0, 1, 2, \ldots,)$ and have a voltage (V^*) separation $\sim 2\omega_w/e$, while the weaker structure has a voltage separation $\sim (\omega_w - \omega_e)/e$. At high field, parity conservation is broken and the voltage separation $\sim \omega_w/e$.

For high magnetic field applied parallel to the long axis of the wire $B \parallel z$, the parity conservation is broken. This may be seen from $I(V)$ for $B = 6\,\text{T}$ (Fig. 7) which shows a series of peaks due to tunneling between states with different symmetry. Among those peaks, the peaks involving the transitions between lowest level in the emitter $(i = 0)$ and the jth state in the well for which $eB\Delta s \sim k_{j,\max}$ $(= [2m(j + \frac{1}{2})\omega_w]^{1/2})$ are found to occur strongly (this is true for $j \sim 5$ at $B = 6\,\text{T}$, see Fig. 7). This is because a high energy simple harmonic oscillator state has a pronounced maximum in $\Phi_j^2(k_y)$ at $k_{j,\max}$. The voltage (V^*) spacing is, therefore, given by ω_w/e for these stronger peaks.

The origin of the high field weak modulation observed for perpendicular field $B \parallel y$, which we do not observe for $\omega_e = 0$, can be explained as follows. Since each occupied emitter subbands has a different Fermi wave vector k_{Fi}, the subband has a different voltage threshold for resonant tunneling. For finite ω_e, for example, of $\varepsilon_F/\omega_e \sim 4$ as was shown in Fig. 6, the difference can be well resolved and seen as the high field weak modulation. We find that the observed structure is mainly due to this difference in the threshold voltage of each occupied emitter subbands together with weak modulation of a period of $2\omega_w/e$ which originated in symmetry of the emitter and the well wave functions along the y direction. We can, therefore, deduce the number of occupied emitter subbands form the high field weak structure.[26]

V. CONCLUSION

We have studied in this paper the tunneling current from a quasi-two- $(\omega_e = 0)$ or quasi-one- $(\omega_e > 0)$ dimensional emitter state into a quantum wire under a magnetic field applied normal to the current direction. The current has been calculated assuming simple harmonic confining potentials within the transfer Hamiltonian formalism.

We have shown that peaks in $I(V)$ due to lateral quantum confinement may be unambiguously identified from their dependence on a high magnetic field oriented perpendicular to the current and parallel to the long axis of the quantum wire. This is due to the fact that the pronounced maxima in the matrix elements of $\Phi_j^2(k_y)$ at around the classical turning points are the only features in $\Phi_j^2(k_y)$ for higher energy states. On the other hand, for a weak magnetic field, the matrix elements involved have several pronounced peaks which result in the complex behavior of $I(V)$.

For a magnetic field applied perpendicular to the long axis of the quantum wire, we have found that the high field weak modulation arises from the formation of 1D subbands in the emitter. This may be used to deduce the number of occupied emitter subbands. For zero field, two

series of peaks has been identified: a strong series which is due to a resonance over several well states, and a weak series of peaks which corresponds to the individual peak of the matrix elements $\Phi_j^2(k_y)$ for $\omega_e = 0$, or individual transitions between discrete emitter and well states for $\omega_e \gtrsim \Gamma$.

ACKNOWLEDGMENTS

N.M. is grateful to the British Council for financial support. P.H.B. and L.E. are grateful to the Royal Society for financial support. This work was supported by the UK SERC.

* Permanent address: Department of Electronic Engineering, Osaka University, 2-1 Yamada-oka, Suita City, Osaka 565, Japan.

† Present address: Department of Physics, HKUST, Clear Water Bay, Kowloon, Hong Kong.

[1] L.L Chang, L. Esaki, and R. Tsu, Appl. Phys. Lett. **24**, 593 (1974).

[2] M.A. Reed, J.N. Randall, R.J. Aggarwal, R.J. Matyi, T.M. Moore, and A.E. Wetsel, Phys. Rev. Lett. **60**, 535 (1988).

[3] J.N. Randall, M.A. Reed, R.J. Matyi, and T.M. Moore, J. Vac. Sci. Technol. B **6**, 1861 (1988).

[4] S. Tarucha, Y. Hirayama, T. Saku, and T. Kimura, Phys. Rev. B **41**, 5459 (1990).

[5] M. Tewordt, V.J. Law, M.J. Kelly, R. Newbury, M. Pepper, D.C. Peacock, J.E.F. Frost, D.A. Ritchie, and G.A.C. Jones, J. Phys. Condens. Matter **2**, 8969 (1990).

[6] Bo Su, V.J. Goldman, M. Santos, and M. Shayegan, Appl. Phys. Lett. **58**, 747 (1991).

[7] S. Tarucha, Y. Hirayama, and Y. Tokuda, Appl. Phys. Lett. **58**, 1623 (1991).

[8] S. Tarucha, Y. Tokura, and Y. Hirayama, Phys. Rev. B **44**, 13 815 (1991).

[9] M.W. Dellow, P.H. Beton, C.J.G.M. Langerak, T.J. Foster, P.C. Main, L. Eaves, M. Henini, S.P. Beaumont, and C.D.W. Wilkinson, Phys. Rev. Lett. **68**, 1754 (1992).

[10] P. Guéret, N. Blanc, R. Germann, and H. Rothuizen, Phys. Rev. Lett. **68**, 1896 (1992); see also Ref. 14.

[11] P.H. Beton, M.W. Dellow, P.C. Main, T.J. Foster, L. Eaves, A.F. Jezierski, M. Henini, S.P. Beaumont, and C.D.W. Wilkinson, Appl. Phys. Lett. **60**, 2508 (1992).

[12] M.A. Reed, J.N. Randall, and J.H. Luscombe, Semicond. Sci. Technol. **7**, B12 (1992).

[13] P. Guéret, N. Blanc, R. Germann, and H. Rothuizen, Semicond. Sci. Technol. **7**, B462 (1992).

[14] P.H. Beton, L. Eaves, and P.C. Main, Phys. Rev. Lett. **69**, 2995 (1992).

[15] P. Guéret, N. Blanc, R. Germann, and H. Rothuizen, Phys. Rev. Lett. **69**, 2996 (1992).

[16] J-W. Sakai, T.M. Fromhold, P.H. Beton, L. Eaves, M. Henini, P.C. Main, F.W. Sheard, and G. Hill, Phys. Rev. B **48**, 5664 (1993).

[17] S.Y. Chou, E. Wolak, and J.S. Harris, Jr., Appl. Phys. Lett. **52**, 657 (1988).

[18] H.C. Liu and G.C. Aers, Solid State Commun. **67**, 1131 (1988).

[19] G.W. Bryant, Phys. Rev. B **39**, 3145 (1989).

[20] M. Luban, J.H. Luscombe, M.A. Reed, and D.L. Pursey, Appl. Phys. Lett. **54**, 1997 (1989).

[21] H.C. Liu and G.C. Aers, J. Appl. Phys. **65**, 4908 (1989).

[22] G.C. Aers and H.C. Liu, Solid State Commun. **73**, 19 (1990).

[23] G.W. Bryant, Phys. Rev. B **44**, 3064 (1991).

[24] G.W. Bryant, Phys. Rev. B **44**, 3782 (1991).

[25] J-W. Sakai, N. La Scala, Jr., P.C. Main, P.H. Beton, T.J. Foster, A.K. Geim, L. Eaves, M. Henini, G.Hill, and M.A. Pate, Solid-State Electron. **37**, 965 (1994).

[26] J. Wang, P.H. Beton, N. Mori, L. Eaves, H. Buhmann, L. Mansouri, P.C. Main, T.J. Foster, and M. Henini, Phys. Rev. Lett. **73**, 1146 (1994).

[27] J. Wang, P.H. Beton, N. Mori, H. Buhmann, L. Mansouri, L. Eaves, P.C. Main, T.J. Foster, and M. Henini, Appl. Phys. Lett. **65**, 1124 (1994).

[28] See, for example, W.R. Frensley, Rev. Mod. Phys. **62**, 745 (1990).

[29] $\phi_i(\ell; x) = (\sqrt{\pi} 2^i i! \ell)^{-1/2} H_i(x/\ell) \exp[-\frac{1}{2}(x/\ell)^2]$ with H_i being the Hermit polynomial.

[30] G. Ihm, M.L. Falk, S.K. Noh, S.J. Lee, and T.W. Kim, Phys. Rev. B **46**, 15 270 (1992).

[31] M. Jonson, Phys. Rev. B **39**, 5924 (1989).

[32] $\Phi_j(\ell^{-1}; k) = \left[2\pi\ell/(\sqrt{\pi} 2^j j!)\right]^{1/2} H_j(k\ell) \exp[-\frac{1}{2}(k\ell)^2]$.

[33] M.L. Leadbeater, L. Eaves, P.E. Simmonds, G.A. Toombs, F.W. Sheard, P.A. Claxton, G. Hill, and M.A. Pate, Solid-State Electron. **31**, 707 (1988)

[34] S. Ben Amor, K.P. Martin, J.L. Rascol, R.J. Higgins, A. Torabi, H.M. Harris, and C.J. Summers, Appl. Phys. Lett. **53**, 2540 (1988).

[35] J. Smoliner, W. Demmerle, G. Berthold, E. Gornik, G. Weimann, and W. Schlapp, Phys. Rev. Lett. **63**, 2116 (1989).

[36] M.L. Leadbeater, F.W. Sheard, and L. Eaves, Semicond. Sci. Technol. **6**, 1021 (1991).

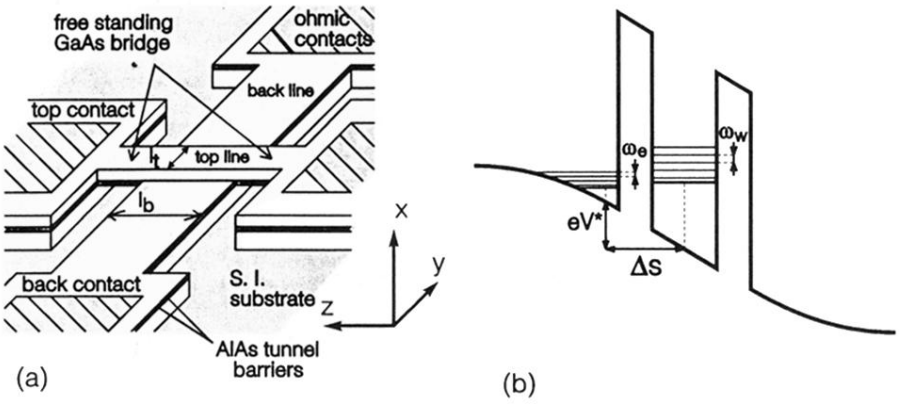

FIG. 1. Schematic diagrams of the GaAs/AlAs resonant tunneling diode (a) and the conduction band profile (b). The active area of the device is the region of overlap of two GaAs bars, one (thickness ℓ_t) etched in the top contact layer and the other (thickness ℓ_b) in the bottom contact layer.

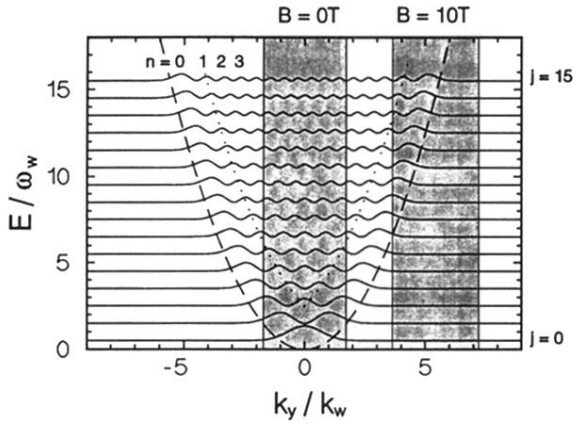

FIG. 3. Plots of probability density $\Phi_j^2(k_y)$ versus k_y for laterally bound states in the quantum well for $j = 0 \sim 15$ (solid lines), the dispersion of the emitter states (broken line), and the locus of the $n = 1$ maxima (dotted line). Also shown (shaded) is the integration range for Eq. (2.15) for $B = 0\,\mathrm{T}$ and $10\,\mathrm{T}$. The horizontal axis is in units $k_w = (m\omega_w)^{1/2}$. There are N $(= [j/2] + 1)$ maxima in $\Phi_j^2(k_y)$ lying in the range of $k_y \leq 0$ (or $k_y \geq 0$) labeled $n = 0, 1, 2, \ldots$, for the $j = 15$ curve.